Journal of Physiology - Paris 103 (2009) 37–45

Contents lists available at ScienceDirect

Journal of Physiology - Paris

journal homepage: www.elsevier.com/locate/jphysparis

Functional geometry of the horizontal connectivity in the primary visual cortex

Alessandro Sarti [a,*], Giovanna Citti [b], Jean Petitot [c]

[a] Università di Bologna, Via Risorgimento 2, Bologna, Italy
[b] Università di Bologna, Piazza di Porta S. Donato 5, Bologna, Italy
[c] CREA, Ecole Polytechnique, 1 rue Descartes, Paris, France

ARTICLE INFO

Keywords:
Horizontal connectivity
Primary visual cortex
Subjective completion
Lie group
Hyperbolic structure

ABSTRACT

We present a geometrical model of the functional architecture of the primary visual cortex. In particular we describe the geometric structure of connections found both in neurophysiological and psychophysical experiments, modeling both co-axial and trans-axial excitatory connections. The model shows what could be the deep structure for both boundary and figure completion and for morphological structures such as the medial axis of a shape.

1. Introduction

It is well known (see Hubel, 1988), that the first layers of the visual cortex present a retinotopic and hypercolumnar structure. The retinotopy means that there exist mappings from the retina to the cortical layers which preserve retinal topography, while the columnar and hypercolumnar structure organizes the cells of V1 in columns corresponding to parameters like orientation, ocular dominance and color.

Recently, this structure has been described with instruments of differential geometry. Hoffman (1989) and Petitot (1994) first modeled the hypercolumnar structure as a fiber bundle. From this point of view the cortex is described as a geometrical structure $V = M \times P$, where M describes the two-dimensional retinal plane, while the secondary variables are described by the fiber P over each point. The structure of the hypercolumns characterizes different families of cells. After that it has been proposed in Citti and Sarti (2006) to model the structure of the odd simple cells in a contact structure in the Lie group of roto-translation, while in Sarti et al. (2008) the set of even complex was described as a symplectic space taking into account scale. Finally Arcozzi et al. (preprint) endowed this space with the structure of an hyperbolic space, which better outline the relation between odd and even simple cells. Other models based on differential geometry in higher dimensional spaces are due to Franken et al. (2007) and Shahar and Zucker (2003).

In this review paper we adopt a general point of view, giving a description of these family of cells in an unitary way, outlining the fact that the mathematical structure which model the different layers of the cortex is the same in these different examples, and the functionality of cells are implemented through analogous neural mechanisms. However, since the dimensionality of the fiber is different in each of the specific examples considered, each family will be responsible of a different completion phenomenon.

We start from the well known observation that the set of simple cells receptive profiles (RPs) is generated by the action of a group of the visual plane on a Gabor mother function. The group will be three- or four-dimensional, depending on the group of cells we are describing. In particular, in case of the odd family of cells, we assume that all RP's are obtained by rotations and translations, while in the even case we consider rotations, dilations and translations. Each hypercolumn of simple cells RP's, defined at a retinal point (x, y), forms a subgroup of the considered group (respectively, of rotations and translations in the two examples). This structure is identically repeated for every point of the retina, and can therefore be considered as a fiber of the cortical principal bundle. Then we show that the neural process of *maxima selection* due to intracortical short range inhibitory connections internal to hypercolumns selects in each case the section of the fibration lifting boundaries in M to curves in V1 and whole figures in M to surfaces in V1.

From the neurophysiological point of view there is evidence of connections between simple cells belonging to different hypercolumns. These neural connections are what neurophysiologists call long range horizontal connections. They implement what geometers call a *connection* operating a *parallel transport* between fibers

* Corresponding author.
E-mail addresses: alessandro.sarti@unibo.it (A. Sarti), citti@dm.unibo.it (G. Citti), petitot@poly.polytechnique.fr (J. Petitot).

0928-4257/$ - see front matter © 2009 Published by Elsevier Ltd.
doi:10.1016/j.jphysparis.2009.05.004

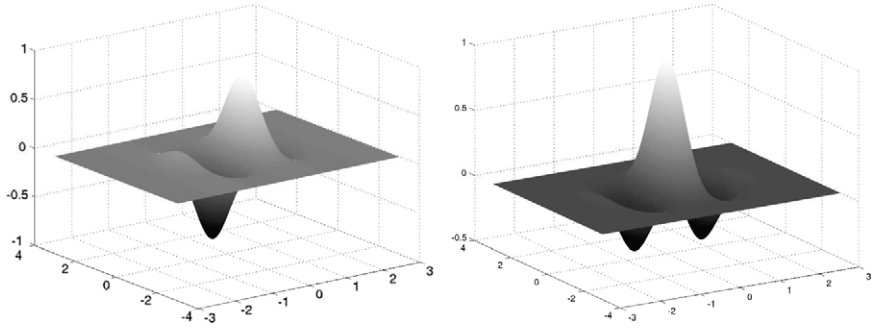

Fig. 1. A representation of the real (left) and imaginary (right) part a Gabor filter.

of a bundle.[1] This latter connection (in the geometric sense) can be expressed in terms of differential part structure, and deeply depends on the dimension of the space.

In the case of odd simple cells, as in Petitot and Tondut (1999) we show the total space V of the fiber bundle modeling V1 is equipped with a natural contact structure neurally implemented by long range horizontal connections. Integral curves of the natural contact structure in the three-dimensional fiber bundle V is a mathematical representation of the*association field* of Field, Hayes and Hess. Due to the fundamental contact structure (making V1 an implementation of the space of 1-jets of curves in M) contour integration can be performed.

In the case of even simple cells, where, as in Sarti et al. (2008) and Arcozzi et al. (preprint) the scale dimension is added, we obtain a four-dimensional structure, which will be considered an hyperbolic structure. In our model here, the integral curves of the four-dimensional structure model more finely the connectivity pattern between simple cells in V1, as observed by electrophysiological experiments. In other words the structure introduces a system of natural coordinates in the four-dimensional space $\mathbb{C}^2$ which is implemented by neural connectivity.[2]

The proposed meaning of the scale variable is the distance from the boundaries of the image. Hence, at scale $\sigma = 0$, we recover the boundaries, only described by the orientation, and we reduce to the previous three-dimensional contact structure. The filtering in the hyperbolic space realizes the well-known propagation of the boundary which gives structure to the interior of the image. The singularities of the propagation generate the so called ?cut locus? or symmetry axis of the shape.

The paper is organized as follows:

- In Section 2 we geometrically model the set of receptive profiles, the hypercolumnar structure and the maximum selection over the fiber.
- In Section 3 we restrict ourselves to the set of odd simple cells, which can be described using only the orientation as an engrafted variable. In particular we outline how the action of this family of cells is responsible for the boundary completion.
- In Section 4 we model the set of even simple cells, responsible for the completion of interior as a hyperbolic space.

2. The receptive profiles

2.1. The set of receptive profiles

The visual plane M will be identified with the plane $\mathbb{R}^2$ endowed with coordinates (x, y) and a fixed frame (∂_x, ∂_y). This is of course a wild idealization and presupposes the choice of an arbitrary global origin $O = (0, 0)$.

When a visual stimulus I of intensity $I(x, y) : M \subset \mathbb{R}^2 \to \mathbb{R}^+$ activates the retinal layer of photoreceptors (identified with the visual field) $M \subset \mathbb{R}^2$, the cells centered at every point (x, y) of M process in parallel the retinal stimulus with their receptive profile (RP) $\Psi_{(x,y)}$, which is defined on M.

Each RP acting on a point (x, y) depends upon a preferred direction θ and a scale σ, and it has been observed experimentally that *the set of simple cells RPs is obtained via translations to the point* (x, y), *rotations of angle* θ, *and dilations of scale* σ *from a unique profile, of Gabor type*.[3] This means that there does exist a mother profile $\Psi_0(\xi, \eta)$ from which all the observed profiles can be deduced by transformation.

A good formula for Ψ_0 seems to be

$$\Psi_0(\xi, \eta) = e^{-(\xi^2+\eta^2)} e^{2i\eta}. \tag{1}$$

In Fig. 1 we represent its odd and even parts which are, respectively, the imaginary and the real parts.

It has to be noted that the RPs $\Psi_{(x,y)}$ are localized in a neighborhood of the point (x, y). Hence, they will be expressed in local coordinates, around the point (x, y), obtained by rotation and dilation of the initial ones. Any vector will then have two representations: coordinates $(\tilde{\xi}, \tilde{\eta})$ in the global frame centered at (0,0), and (ξ, η) in the local frame centered at (x, y):

$$\begin{cases} \xi = \frac{1}{\sigma}((\tilde{\xi} - x)\cos\theta + (\tilde{\eta} - y)\sin\theta), \\ \eta = \frac{1}{\sigma}(-(\tilde{\xi} - x)\sin\theta + (\tilde{\eta} - y)\cos\theta). \end{cases} \tag{2}$$

The factor $\frac{1}{\sigma}$ means that, when $\sigma \to 0$, one zooms in the neighborhood of (x, y). Therefore all the observed profiles can be modeled as

$$\Psi_{x,y,\theta,\sigma}(\tilde{\xi}, \tilde{\eta}) = \frac{1}{\sigma^2} \Psi_0(\xi, \eta).$$

In this model we consider a uniform distribution of orientations and scales, even if there is a neurophysiological evidence of covariation of scale and orientation (Issa et al., 2000).

We recall that a change of frames can act on the space M or, by duality, on functions defined on M. Precisely, if A is a linear transformation of M, it transforms also functions ψ through the formula

[1] It must be emphasized that the technical lexicons of neurophysiology and geometry use the same terms "fibers", "connections", etc., in completely different ways. In general the context will eliminate any ambiguity.

[2] $\mathbb{C}^2$ is two-dimensional over $\mathbb{C}$ but four-dimensional over $\mathbb{R}$.

[3] In a preceding paper (Sarti et al., 2008) we used an exponential scale $s = e^{\sigma}$. But for reasons explained later it is better to use a logarithmic scale σ.

$$A\psi(\tilde{\xi},\tilde{\eta}) = \frac{1}{det(A)}\psi(A^{-1}(\tilde{\xi},\tilde{\eta})).$$

Accordingly we will denote $A^{-1}_{x,y,\theta,\sigma}$ the transformation defined in (2), and obtain

$$\Psi_{x,y,\theta,\sigma}(\tilde{\xi},\tilde{\eta}) = (A_{x,y,\theta,\sigma}\Psi_0)(\tilde{\xi},\tilde{\eta}).$$

The expression of A thus becomes:

$$A_{x,y,\theta,\sigma}(\xi,\eta) = \begin{pmatrix} x \\ y \end{pmatrix} + \sigma \begin{pmatrix} \cos(\theta) & -\sin(\theta) \\ \sin(\theta) & \cos(\theta) \end{pmatrix} \begin{pmatrix} \xi \\ \eta \end{pmatrix}.$$

Notice that for simplicity we identify translations in the retinal plane and translations in the cortical layers, neglecting the conformal log-polar retino-cortical mapping. Anyway, the mapping can be taken into account by introducing a suitable metric on cortical layers.

2.2. The output of receptive profiles

The overall output O of the parallel filtering is given by the integral of the signal $I(x,y)$ times the bank of filters:

$$\begin{aligned} O_{(\theta,\sigma)}(x,y) &= \int_M I(\tilde{\xi},\tilde{\eta})\Psi_{(x,y,\theta,\sigma)}(\tilde{\xi},\tilde{\eta})d\tilde{\xi}d\tilde{\eta} \\ &= \int_M I(\tilde{\xi},\tilde{\eta})\Psi_0(A^{-1}_{x,y,\theta,\sigma}(\tilde{\xi},\tilde{\eta}))\frac{d\tilde{\xi}d\tilde{\eta}}{\sigma^2}. \end{aligned} \quad (3)$$

Performing a change of variable with respect to the transformation A, we get:

$$O_{(\theta,\sigma)}(x,y) = \int \Psi_0(\xi,\eta)I(A_{(x,y,\theta,\sigma)}(\xi,\eta))d\xi d\eta.$$

We explicitly note that the linear transformation A acts on the retinal plane M, argument of I. On the contrary the inverse transformation A^{-1} acts on the domain of Ψ_0. This allows us to interpret the domain of Ψ_0 as dual plane, with respect to the retinal plane.

2.3. The hypercolumnar structure

The hypercolumnar structure organizes the cells of V1 in hypercolumns covering a small chart of the visual field (their receptive field) and corresponding to parameters such as orientation, scale, ocular dominance, direction of movement or color for a fixed retinal position (x,y). The hypercolumnar organization means therefore essentially that to each position (x,y) of the retina M is associated a full exemplar $P_{(x,y)}$ of the space of such "secondary" variables.

For each family of engrafted variables, the set of all receptive profiles is obtained from a fixed one by suitable motion, as rotation, dilation, or translation $A_{(\theta,\sigma)}$. So that the set of filters over the point (x,y) becomes:

$$\begin{aligned} RP_{(x,y)} &= \{\Psi_{(x,y,\theta,\sigma)} : (x,y) \text{ fixed}, (\theta,\sigma) \text{ variable}\} \\ &= \left\{A_{(\theta,\sigma)}\Psi_{(x,y,0,0)} : (\theta,\sigma) \in S^1 \times \mathbb{R}\right\}, \end{aligned}$$

where $A_{(\theta,\sigma)} = A_{(0,0,\theta,\sigma)}$.

2.4. Maximal selectivity and geometrical interpretation of lifting

We come now to one of our central points. Up to now we have described the hypercolumnar structure in terms of differential geometry. Now we introduce the functionality of hypercolumns and particularly the orientation and scale *selectivity*.

In the past years several models have been presented to explain the emergence of orientation and scale selectivity in the primary visual cortex. These models use different combinations of feedforward (thalamic) and feedback (intracortical) inputs and consider different involvements of excitatory and inhibitory short range connections (Miller et al., 2001; Worgotter and Koch, 1991; Carandini and Ringach, 1997; Bar et al., 1995; Priebe et al., 1998; Shelley et al., 2000; Nelson et al., 1995). Even if the basic mechanism producing strong orientation selectivity is controversial ("push-pull" models (Miller et al., 2001; Priebe et al., 1998), "emergent" models (Nelson et al., 1995), "recurrent" models (Shelley et al., 2000), only to cite a few), nevertheless it is evident that the intracortical circuitry is able to filter out all the spurious directions and to strictly keep the direction of maximum response of the simple cells.

Neurophysiologically, orientation and scale selectivity is the action of intracortical short range connections to select the maximum response from the output:

$$\begin{aligned} O_{(\theta,\sigma)}(x,y) &= \int_M I(\tilde{\xi},\tilde{\eta})\Psi_{(x,y,\theta,\sigma)}(\tilde{\xi},\tilde{\eta})d\tilde{\xi}d\tilde{\eta} \\ &= \int_M \Psi_0(\xi,\eta)I(A_{(x,y,\theta,\sigma)}(\xi,\eta))d\xi d\eta. \end{aligned}$$

This maximal selectivity is the simplest mechanism (winner-take-all strategy) to accomplish the selection among all different cell responses to effect a lift in the space of features. Given an input I, the neural processing associates to each point (x,y) of the retina M a point $(x,y,\bar{\theta},\bar{\sigma})$ in the cortex.[4] We interpret this mechanism as a lifting into the fiber of the parameter space $\mathbb{R}^2(x,y) \times S^1(\theta) \times \mathbb{R}(\sigma)$ over (x,y). Precisely, the odd part of the filters $\Psi_{(x,y,\theta,\sigma)}$ lifts the boundaries of the image and the even part of the filters lifts the interior of the objects.

We will denote $(\bar{\theta},\bar{\sigma})$ the points of maximal response:

$$O(x,y,\bar{\theta},\bar{\sigma}) = \max_{(\theta,\sigma)} O(x,y,\theta,\sigma). \quad (4)$$

This maximality condition can be mathematically expressed requiring that the gradient of O with respect to the variables (θ,σ) vanishes at the point $(x,y,\bar{\theta},\bar{\sigma})$:

$$\nabla^{(\theta,\sigma)}O(x,y,\bar{\theta},\bar{\sigma}) = 0.$$

We will also require that at the maximum point the Hessian is strictly negatively definite:

$$Hess(O) < 0.$$

2.5. Odd and even RP's

We will study separately the real and the imaginary part of the filter, which models, respectively, the even and the odd simple cells of the visual cortex. Both sets of filters have similar geometrical structure, described trough the hypercolumnar structure and the corresponding fiber bundle structure. In both sets of cells the intracolumnar connectivity is responsible for the phenomena of orientation and scale selectivity, but the two families of cells have different shapes. Hence, even though they act in the same way on the input, they are able to detect different features. Indeed the odd cells will be responsible for boundary detection, and the even ones for the object detection.

3. The odd RP's

Boundary detection is performed by odd simple cells that maximally fires at discontinuity of the stimulus. For simplicity in this section we will consider an unitary value of the scale, taking into account only the position and orientation of the RP (see Fig. 2).

[4] A "point" in the cortex means a neuron or a small assembly of neurons acting as a neuron.

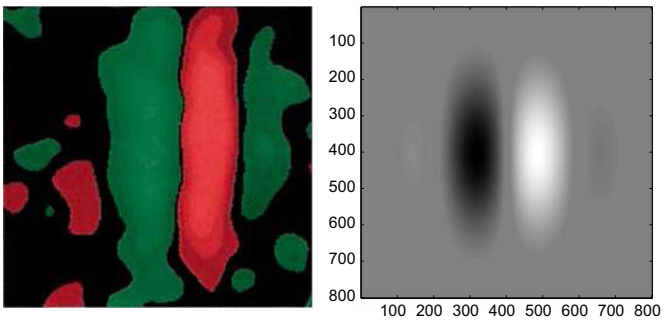

Fig. 2. In vivo registered odd receptive field (left, from (De Angelis et al., 1995)) and a schematic representation of it as a Gabor filter (right).

The odd part of the filter can be locally approximated (up to a multiplicative constant) as

$$\sin(2\tilde{\eta})exp(-(\tilde{\xi}^2+\tilde{\eta}^2)) \simeq 2\tilde{\eta}exp(-(\tilde{\xi}^2+\tilde{\eta}^2)) = -\partial_{\tilde{\eta}}exp(-(\tilde{\xi}^2+\tilde{\eta}^2)).$$

3.1. The monodimensional fiber $RP_{(x,y)}$ over each retinal point (x,y)

Since we assume that the scale is fixed, the hypercolumns introduced in Section 2.3 contains only one feature, and are modelled as monodimensional fibers. To every fixed point (x,y) of the retinal plane M is associated the complete set of values for orientation θ. In other words, for (x,y) fixed, we consider all filters obtained via rotations of an angle θ from a fixed one $\Psi_{(x,y,0)}$, so that the set of filters over the point (x,y) becomes:

$$RP_{(x,y)} = \{\Psi_{(x,y,\theta)} : (x,y) \text{ fixed, } \theta \text{ variable}\} = \left\{A_{(\theta,\sigma)}\Psi_{(x,y,0,0)} : (\theta,\sigma) \in S^1 \times \mathbb{R}\right\},$$

where we have again denoted $A_{(\theta,\sigma)} = A_{(0,0,\theta,\sigma)}$.

A derivative in the direction $\tilde{\eta}$ can be expressed in the original variables (x,y,θ) as a directional derivative in the direction of the vector $X_3 = (-\sin(\theta),\cos(\theta))$. We will denote it

$$X_3 = -\sin(\theta)\partial_x + \cos(\theta)\partial_y. \quad (5)$$

This derivative, applied to a function I, expresses the projection of the gradient in the direction $(-\sin(\theta),\cos(\theta))$.

Hence a hypercolumn is modelled as a fiber of RPs and its action on the image is a fiber of directional derivations for every orientation θ (see Fig. 3).

3.2. Orientation selectivity and "nonmaximal" suppression

The intracortical circuitry is able to filter out all the spurious directions and to strictly keep the direction of maximum response of the simple cells. Since $X_3 I$ is the projection of the gradient in the direction of the vector $(-\sin(\theta),\cos(\theta))$, the maximum will be achieved at a value $\bar{\theta}$, which is the direction of the gradient.

Then, if we call $\bar{\theta}$ the point of maximum, condition (4) reduces to

$$|X_3(\bar{\theta})I| = \max_{\theta}|X_3(\theta)I|. \quad (6)$$

Proposition 3.1. *The point of maximum over the fiber is attained at the value* $\bar{\theta}$ *of the orientation of image level lines. In other words the vector*

$$X_1 = \cos(\bar{\theta})\partial_x + \sin(\bar{\theta})\partial_y$$

is parallel to the level lines at the point (x,y).

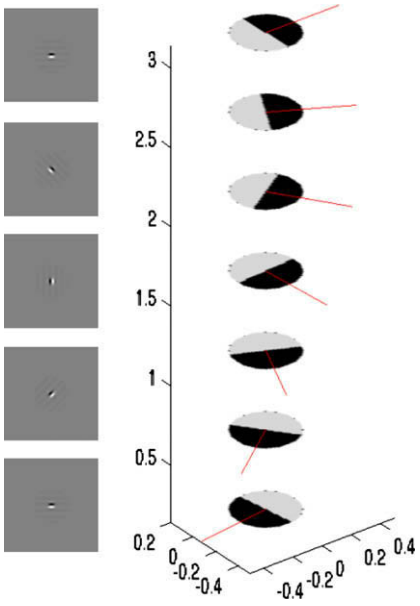

Fig. 3. Odd part of Gabor filters with different orientations (left) and schemata of odd simple cells arranged in a hypercolumn of orientations.

Indeed at the maximum point $\bar{\theta}$ the derivative with respect to θ vanishes, and we have

$$0 = \frac{\partial}{\partial\theta}X_3(\bar{\theta})I = -X_1(\bar{\theta})I = -\langle X_1(\bar{\theta}), \nabla I\rangle.$$

This implies that X_1 is orthogonal to the gradient, so that it has the direction of the level lines of I.

3.3. The contact structure

As a direct consequence of the preceding assertion we can deduce that the lifted curves are tangent to the plane generated by the vectors X_1 and X_2.

In the standard Euclidean setting, the tangent space to $\mathbb{R}^2 \times S^1$ has dimension 3 at every point. Here we have selected a section X_3 of the tangent space. This defines also a bi-dimensional subset of the tangent space at every point, orthogonal to $X_3(\theta)$. This is called the *contact plane* (see Fig. 4). It is generated by

$$X_1(\theta) = (\cos(\theta),\sin(\theta),0), \quad X_2 = (0,0,1)$$

and can be represented as

$$\pi_{x,y,\theta} = \{\alpha_1 X_1 + \alpha_2 X_2 : \alpha_1,\alpha_2 \in \mathbb{R}\}.$$

This plane is the kernel of the 1-form

$$\omega_3 = -\sin(\theta)dx + \cos(\theta)dy.$$

Proposition 3.2. *The 1-form* ω_3 *is a contact form.*

Indeed a direct computation shows that

$$d\omega_3 = (\cos(\theta)dx + \sin(\theta)dy) \wedge d\theta.$$

In other words the 2-form $d\omega_3$ spans the contact plane. Since ω_3 is orthogonal to this plane, then

$$\omega_3 \wedge d\omega_3$$

is the volume form of the space, which implies that ω_3 is a contact form.

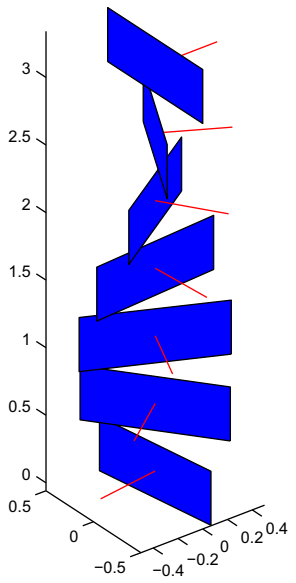

Fig. 4. The contact planes at every point, and the orthogonal vector X_3.

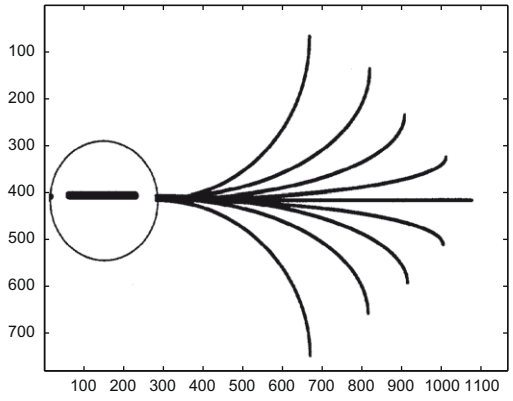

Fig. 5. Association field from the experiment of Field et al. (1993).

3.4. Association fields and integral curves

The lifted points of the image would remain without relations between them without an integrative process allowing to connect local tangent vectors and to form integral curves. This process is at the base of both regular contours and illusory contours formation (Petitot and Tondut, 1999).

The most plausible model of connections is based on a mechanism of "local induction". The specificity of this local induction is described by the association field (Field et al., 1993).

The local association field is shown in (Fig. 5) and it can be interpreted as a family of integral curves of vector fields belonging to the contact planes spanned by X_1 and X_2, and starting at a fixed point (x, y, θ):

$$\gamma'(t) = X_1(\gamma) + kX_2(\gamma), \quad \gamma(0) = (x, y, \theta) \tag{7}$$

obtained by varying the parameter k in $\mathbb{R}$ (Fig. 6). This parameter k expresses the curvature of the projection of the curve γ on the plane (x, y) (see Citti and Sarti, 2006; Petitot, 1994). Such a curve tangent to the contact planes at every point, is called an *integral curve* and, when k is constant, is given by the formula

$$\gamma(t) = \exp(t(X_1 + kX_2))(x, y, \theta).$$

Note that the coefficient of X_1 never vanishes in this representation, since the projection on the two-dimensional plane (x, y) of an integral curve of X_2 would be a point.

Choosing the Euclidean metric making $\{X_1, X_2\}$ an orthonormal basis in the contact planes, we can set

$$\|X_1 + kX_2\|_E = \sqrt{1 + k^2},$$

so that we can call length of any curve γ expressed as in (7)

$$\lambda(\gamma) = \int_0^1 \|\gamma'(t)\| dt = \int_0^1 \sqrt{1 + k^2}.$$

Consequently it is possible to define

$$d((x, y, \theta), (\bar{x}, \bar{y}, \bar{\theta})) = \inf\{\lambda(\gamma) : \gamma \text{ is an integral curve connecting } (x, y, \theta) \text{ and } (\bar{x}, \bar{y}, \bar{\theta})\}, \tag{8}$$

connecting (x, y, θ) and $(\bar{x}, \bar{y}, \bar{\theta})$

see Nagel et al. (1985). In the Euclidean case the infimum is realized by a geodesic that is a segment. Also here there exists an integral path on which the infimum is achieved, called a geodesic. The geometry so defined is called *sub-Riemannian*.

We will see in the next section that we are mainly interested in surface completion. It is well known (see Hladky and Paul, submitted for publication) that a surface is foliated by a special type of geodesics, namely the geodesics represented as in (7), with constant coefficients.

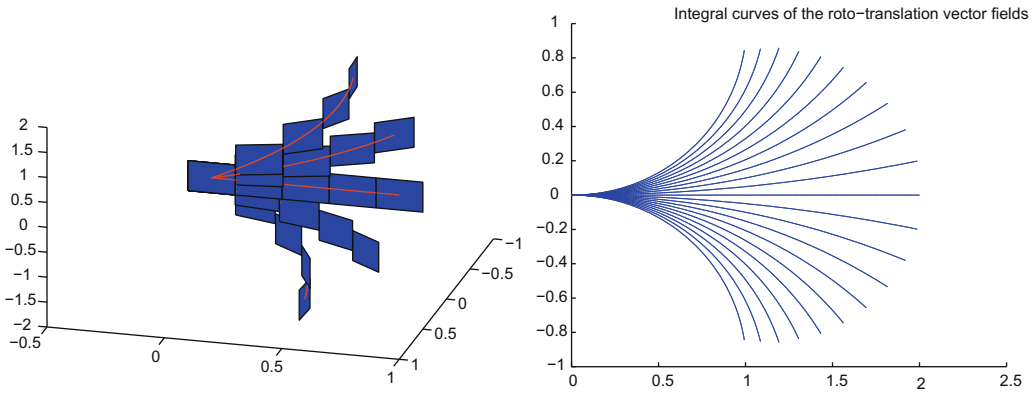

Fig. 6. Integral curves of the field by varying the parameter k. On the left a 3D representation with contact planes is shown, in the right its projection onto the image plane is visualized.

3.5. Lifting of the surface, and selection of geodesics which belong to a surface

The orientation selectivity process we have just described lifts each point (x,y) in the 2D domain of the image to a 3D-point $(x,y,\bar{\theta})$.

If we denote $T_{(x,y)}(\mathbb{R}^2)$ the tangent space to $\mathbb{R}^2$ at the point (x,y), the vector $(-\sin(\bar{\theta}),\cos(\bar{\theta})) \in T_{(x,y)}(\mathbb{R}^2)$ is lifted to the vector field

$$X_3(\bar{\theta}) = (-\sin(\bar{\theta}),\cos(\bar{\theta}),0) \in T_{(x,y,\theta)}(\mathbb{R}^2 \times S^1).$$

The whole image domain is lifted to:

$$\Sigma_0 = \{(x,y,\bar{\theta}) : |X_3(\bar{\theta})I_s| = \max_{\theta} |X_3(\theta)I| > 0\}. \quad (9)$$

This lifted set corresponds to the maximum of activity of the output of the simple cells, that can be modeled as a Dirac mass concentrated on Σ_0 itself, with a density u_0, given by the value of the activity:

$$u_0(x,y,\theta) = O(x,y,\bar{\theta})\delta_\Sigma. \quad (10)$$

4. The even simple cells

The even simple cells are the real part of the mother Gabor filter, so that they are expressed as (see Fig. 7)

$$\cos(2\eta)e^{-(\xi^2+\eta^2)}.$$

The structure of the even simple cells is formally analogous to the set of odd cells, but we will show that it builds a symplectic, instead of a contact structure.

4.1. The two-dimensional fiber $RP_{(x,y)}$ over each retinal point (x,y)

In order to describe the even cells, as before, we associate to every fixed point (x,y) of the retinal plane M a complete set of values for orientation θ and scale σ, i.e. a two-dimensional fiber:

$$RP_{(x,y)} = \{\Psi_{(x,y,\theta,\sigma)} : (x,y) \text{ fixed}, (\theta,\sigma) \text{ variable}\} = \left\{A_{(\theta,\sigma)}\Psi_{(x,y,0,0)} : (\theta,\sigma) \in S^1 \times \mathbb{R}\right\},$$

with $A_{(\theta,\sigma)} = A_{(0,0,\theta,\sigma)}$ (see Fig. 8).

4.2. Orientation-scale selectivity and "nonmaximal" suppression

As in the case of odd cells, again we model the selectivity mechanism as a nonmaximal suppression mechanism. Given an input I, the neural processing associates to each point (x,y) of the retina M a point $(x,y,\bar{\theta},\bar{\sigma})$ in the cortex, We interpret this mechanism as a lifting into the fiber of the parameter space $\mathbb{R}^2(x,y) \times S^1(\theta) \times \mathbb{R}(\sigma)$ over (x,y).

In this geometrical setting, the geometrical meaning of the maximum selectivity mechanism is different from before.

Theorem 4.1 (see Sarti et al., 2008). *At first order approximation, for any fixed value of (x,y), the output function $O(x,y,\theta,\sigma)$ reaches a local maximum at the point $\bar{\theta}$, $\bar{\sigma}$, where $d(\bar{\sigma}) = \frac{1}{\sqrt{2}}\bar{\sigma}$ denotes the distance of (x,y) from the nearest boundary of the image I, and $\bar{\theta}$ denotes the orientation of this boundary at the point where the distance is achieved.*

This theorem ensures that the simple cell selects the couple $(\bar{\theta},\bar{\sigma})$ in such a way that, X_3 being the vector

$$X_3 = -\sin(\bar{\theta})\partial_x + \cos(\bar{\theta})\partial_y, \quad (11)$$

then $(x,y) + \frac{\bar{\sigma}}{\sqrt{2}}X_3$ belongs to the nearest boundary of I (see Fig. 9).

4.3. A symplectic 2-form

In order to take into account the role of the contact structure, we will endow the space $\mathbb{R}^2(x,y) \times S^1(\theta) \times \mathbb{R}(\sigma)$ with a symplectic structure. We multiply ω by the scale factor σ^{-1} (remember it means that, when $\sigma \to 0$, one zooms in the neighborhood of (x,y))

$$\omega = \sigma^{-1}(-\sin(\theta)dx + \cos(\theta)dy).$$

Then we take as symplectic form the 2-form $d\omega$ obtained by differentiating ω with respect to all its variables. The symplectic 2-form $d\omega$ writes:

$$\begin{aligned} d\omega &= \sigma^{-1}(\cos(\theta)dx + \sin(\theta)dy) \wedge d\theta + \sigma^{-2}(-\sin(\theta)dx + \cos(\theta)dy) \\ &\quad \wedge d\sigma \\ &= \sigma^{-1}\omega_1 \wedge \omega_2 + \sigma^{-2}\omega_3 \wedge \omega_4, \end{aligned}$$

where ω_i is the dual form of X_i. This form can be identified with the *left invariant* 2-form deduced by left translations from the standard 2-form on G at 0:

$$dx \wedge d\theta + dy \wedge d\sigma.$$

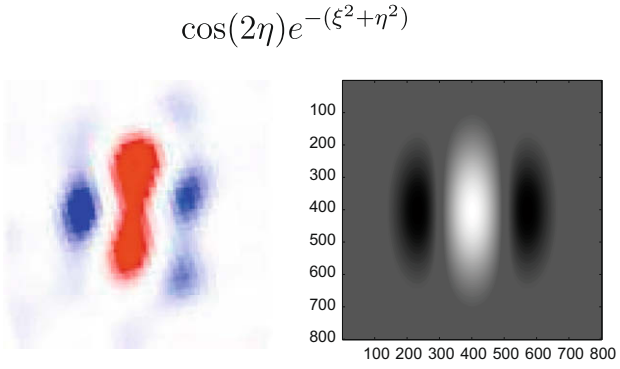

Fig. 7. In vivo registered even receptive field (left – from Niell and Stryker (2008)) and a schematic representation of it as a Gabor filter (right)). Positive sign is in white and negative in black.

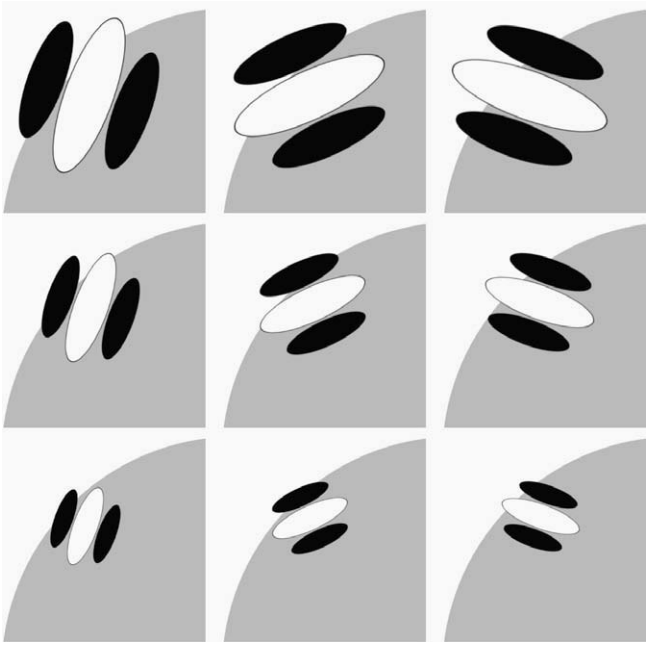

Fig. 8. The two-dimensional fiber of even simple cells, obtained via rotation and dilation of the mother filter.

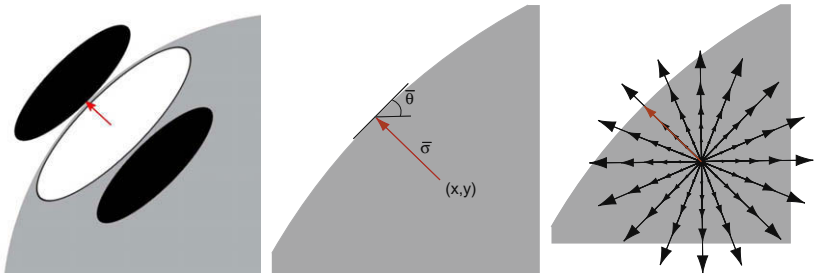

Fig. 9. The simple cell centered in (x,y) takes the maximal activity $O(x,y,\bar{\theta},\bar{\sigma}) = \max_{(\theta,\sigma)} O(x,y,\theta,\sigma)$ at a point $\bar{\sigma}$ which is, up to a constant, the logarithm of the distance to the nearest boundary and $\bar{\theta}$ is the direction of this boundary.

4.4. The hyperbolic structure

We can now adapt the vector fields previously chosen to the structure of the 2-form we have found, following an idea first introduced by (Arcozzi et al., preprint). We will choose the following vector fields

$$\begin{cases} X_1 = \cos(\theta)\partial_x + \sin(\theta)\partial_y \\ X_2 = \partial_\theta \\ X_3 = -\sin(\theta)\partial_x + \cos(\theta)\partial_y \\ X_4 = \partial_\sigma \end{cases}$$

and define a metric G which makes

$$\sigma X_1, \quad \sigma X_2, \quad \sigma^2 X_3, \quad \sigma^2 X_4$$

orthonormal.

Accordingly, the inverse of the metric can be immediately computed as

$$\begin{aligned}(\partial_x,\partial_y,\partial_\theta,\partial_s)^T G^{-1}(\partial_x,\partial_y,\partial_\theta,\partial_s) &= \sigma^2 X_1^2 + \sigma^2 X_2^2 + \sigma^4 X_3^2 + \sigma^4 X_4^2 \\ &= \sigma^2\cos^2(\theta)\partial_x^2 + \sigma^2\sin^2(\theta)\partial_y^2 + 2\sigma^2 \\ &\quad\times \cos(\theta)\sin(\theta)\partial_x\partial_y + \sigma^4 \\ &\quad\times \cos^2(\theta)\partial_x^2 + \sigma^4\sin^2(\theta)\partial_y^2 - 2\sigma^4 \\ &\quad\times \cos(\theta)\sin(\theta)\partial_x\partial_y + \sigma^2\partial_\theta^2 \\ &\quad + \sigma^4\partial_\sigma^2.\end{aligned}$$

Let us now rescale the vector fields, in order to better understand the structure of the space. In this way we can consider the vector fields:

$$X_1, \quad X_2, \quad \sigma X_3, \quad \sigma X_4.$$

It is evident that the scale variable assign a different role to the plane generated by X_1 and X_2 with respect to the plane generated by X_3 and X_4. Indeed, if the scale is small, the tangent space reduces to the plane generated by X_1 and X_2, if the scale is 1, the tangent space is generated by all vector fields, while for large values of the scale, the vectors σX_3, and σX_4 are predominant.

Let us now fix the value of σ, and consider the metric induced on the 3D space (x,y,θ). If σ is constantly equal to 0 the metric reduces to the sub-Riemannian one, and the structure is the contact structure previously studied. Since σ expresses the distance from the boundary, this means that, on the boundaries, the metric is sub-Riemannian, since we have a preferred direction of the diffusion of the visual signal.

If we consider the $3D$ space obtained for σ fixed, but different from 0, we obtain a Riemannian metric, and, for $\sigma = 1$, an Euclidean one. This reflects the fact that, far from the boundaries there is no preferred direction for the diffusion.

In particular, varying σ, we have obtained a foliation of the symplectic structure in $3D$ Riemannian spaces, which tends to the sub-Riemannian one, when σ goes to 0.

This structure models an hyperbolic one (see Fig. 10).

4.5. Integral curves of special vector fields

Let us compute the integral curves of the renormalized vectors,

$$\begin{aligned}\gamma'(t) &= X_1(\gamma(t)) + k_2 X_2(\gamma(t)) + k_3\sigma X_3(\gamma(t)) \\ &\quad + k_4\sigma X_4(\gamma(t)), \quad \gamma(0) \\ &= (x_0, y_0, \theta_0, \sigma_0).\end{aligned} \tag{12}$$

As before we first fix the value of σ. This can be obtained choosing $k_3 = 0$.

If the starting value of σ is $\sigma = 0$, we reduce to the integral curves of the contact structure

$$\gamma'(t) = X_1(\gamma(t)) + k_2 X_2(\gamma(t)), \quad \gamma(0) = (x_0, y_0, \theta_0, 0). \tag{13}$$

The projection on the (x,y) plane is then either a line (if $k_2 = 0$), or a circle of radius $1/k_2$ tangent to the x axis (see Fig. 11 left). The emergence of curvature in this context is strictly related to the curve detection model based on curvature in Parent and Zucker (1989).

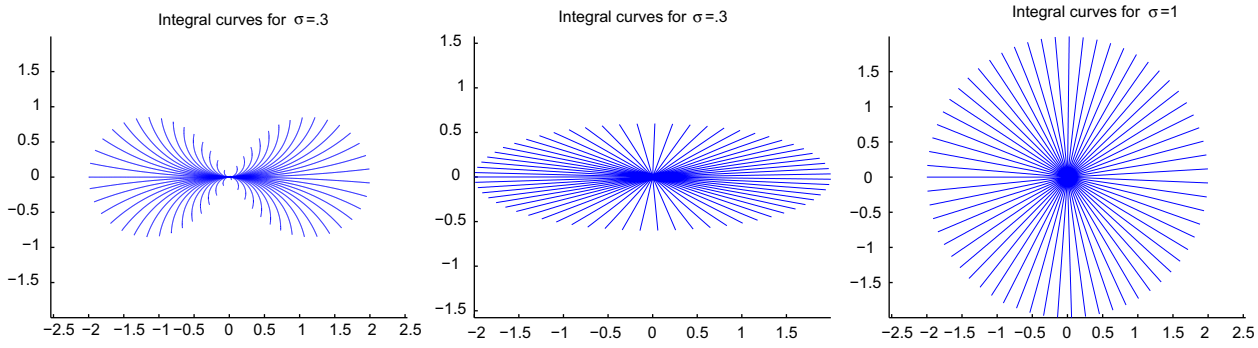

Fig. 10. The 2D-projection of integral curves for $\sigma = 0$, $\sigma = 1/2$, and $\sigma = 1$.

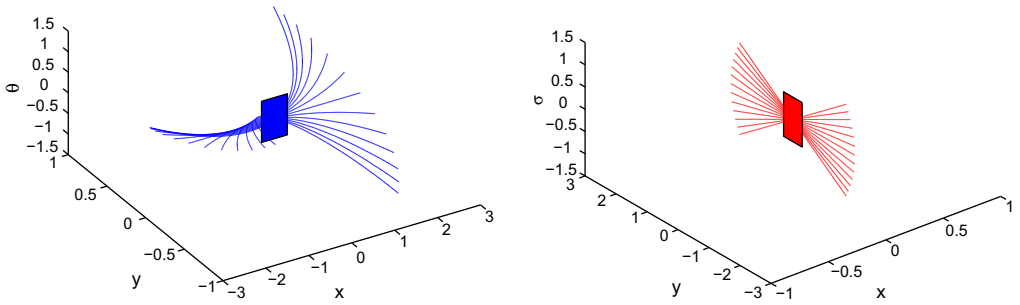

Fig. 11. Integral curves, respectively, of the (X_1, X_2) and (X_3, X_4) vector fields.

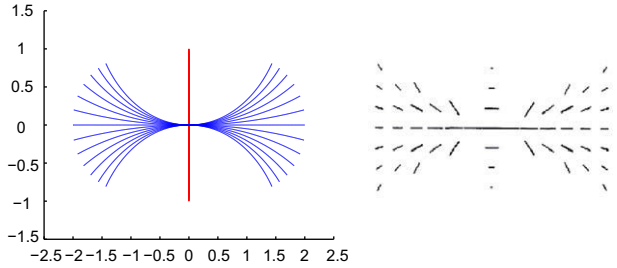

Fig. 12. The projection of the integral curves of the symplectic structure on the retinal plane (left) reveals the pattern of co-axial and trans-axial connections found by neurophysiological experiments (right, from Yen and Finkel (1998)).

If the starting value of $\sigma \neq 0$, we obtain we obtain a new set of curves by varying k_3, and assuming $k_2 = 0$. The projection of these curves on the 2D retinal plane describes an ellipsis, as depicted in Fig. 4.

At small scale the most significant curves are the ones on the plane X_1, and X_2. On the contrary, if the scale is big, the significant ones are the integral curves of the vector fields $X_3 + k_4 X_4$ (we may take $k_3 = 1$ if $k_3 \neq 0$). Hence we obtain:

$$\gamma'(t) = X_3(\gamma(t)) + k_4 X_4(\gamma(t)), \quad \gamma(0) = (x, y, \theta, \sigma). \tag{14}$$

The curves cross the foliation. Their projection on the (x, y) plane is orthogonal to the direction θ_0. For k variable the integral curve is the line of slope k in the fixed "vertical" plane $\{X_3, X_4\}$ (see Fig. 11 right).

The projection of these two classes of integral curves on the base plane (x, y) is plotted in Fig. 12. Their pattern is in good agreement with the pattern of long range connections found both in neurophysiological and psychophysical experiments. In fact, excitatory connections are confined to two regions, one flaring out along the axis of orientation of the cell (co-axial), and another confined to a narrow zone extending orthogonally to the axis of orientation (trans-axial, vertical). The co-axial connections are exactly the same we found in the previous section. The symplectic model adds *a second set of trans-axial excitatory connections* which extends orthogonally from the orientation axis of the cell. There is anatomical evidence consistent with the existence of these orthogonal connections (Fitzpatrick, 1996; Lund et al., 1985; Mitchinson and Crick, 1982; Rockland and Lund, 1982, 1983). The trans-axial connections are represented here as integral curves of the fields X_3, X_4. The reason why co-axial connections spread out in a fan, while trans-axial connections are more spatially focused is that the roto-translation fields X_1, X_2 not only do not commute but their commutator is linearly independent from them:

$$[X_1, X_2] = -X_3,$$

while the vectors X_3, X_4 do not commute but their commutator is linearly dependent upon them:

$$[X_3, X_4] = -X_3.$$

Then integral curves of roto-translation fields are not planar (Fig. 12, left) while integral curves of X_3, X_4 belong to a plane (Fig. 12, right) whose projection on the (x, y) plane is just a line (vertical line[5] Fig. 12).

References

Arcozzi, N., Citti, G., Sarti, A., preprint. Association fields of simple cells as parallel transport in a hyperbolic symplectic structure.

Bar, O., Sompolinsky, H., Ben-Yishai, R., 1995. Theory of orientation tuning in visual cortex. PNAS 92, 3844–3848.

Ben-Shahar, O., Zucker, S., 2003. Geometrical computations explain projection patterns of long-range horizontal connections in visual cortex. Neural Comput. 16 (3), 445–476.

Carandini, M., Ringach, D.L., 1997. Predictions of a recurrent model of orientation selectivity. Vision Res. 37, 3061–3071.

Citti, G., Sarti, A., 2006. A cortical based model of perceptual completion in the Roto-translation space. J. Math. Imaging Vision 24 (3), 307–326. 20.

De Angelis, G.C., Ozhawa, I., Freeman, R.D., 1995. Receptive-field dynamics in the central visual pathways. Trends Neurosci. 18 (10), 451–458.

Field, D.J., Hayes, A., Hess, R.F., 1993. Contour integration by the human visual system: evidence for a local association field. Vision Res. 33, 173–193.

Fitzpatrick, D., 1996. The functional organization of local circuits in visual cortex: insights from the study of tree shrew striate cortex. Cereb. Cortex 6, 329–341.

Franken, Erik, Duits, Remco, ter Haar Romeny, Bart M., 2007. Nonlinear diffusion on the 2d euclidean motion group. In: Sgallari, Fiorella, Murli, Almerico, Paragios, Nikos (Eds.), SSVM, Lecture Notes in Computer Science, vol. 4485. Springer, pp. 461–472.

Hladky, R., Pauls, S., submitted for publication. Minimal surfaces in the roto-translation group with applications to a neuro-biological image completion model.

Hoffman, W.C., 1989. The visual cortex is a contact bundle. Appl. Math. Comput. 32, 137–167.

Hubel, D.H., 1988. Eye, Brain and Vision. Scientific American Library.

Issa, N.P., Trepel, C., Stryker, M.P., 2000. Spatial frequency maps in cat visual cortex. J. Neurosci. 20, 8504–8514.

Lund, J., Fitzpatrick, D., Humphrey, A.L., 1985. The striate visual cortex of the tree shrew. In: Jones, E.G., Peters, A. (Eds.), Cerebral Cortex. Plenum, New York, pp. 157–205.

Miller, K.D., Kayser, A., Priebe, N.J., 2001. Contrast-dependent nonlinearities arise locally in a model of contrast-invariant orientation tuning. J. Neurophysiol. 85, 2130–2149.

Mitchinson, G., Crick, F., 1982. Long axons within the striate cortex: their distribution orientation and patterns of connections. PNAS 79, 3661–3665.

Nagel, A., Stein, E.M., Wainger, S., 1985. Balls and metrics defined by vector fields I: basic properties. Acta Math. 155, 103–147.

Nelson, S.B., Sur, M., Somers, D.C., 1995. An emergent model of orientation selectivity in cat visual cortical simples cells. J. Neurosci. 15, 5448–5465.

Niell, Cristopher M., Stryker, Michael P., 2008. Highly selective receptive fields in mouse visual cortex. J. Neurosci. 28 (30), 7520–7536 (July 23).

Parent, P., Zucker, S.W., 1989. Trace interference, curvature consistency and curve detection. IEEE Trans. Pattern Anal. Machine Intel. 11, 823–839.

[5] For interpretation of color in Figs. 2–4, 6, 7 and 9–12 the reader is referred to the web version of this article.

Petitot, J., 1994. Phenomenology of perception qualitative physics and sheaf mereology. In: Proceedings of the 16th International Wittgenstein Symposium, Vienna, Verlag Hlder-Pichler-Tempsky, pp. 387–408.

Petitot, J., Tondut, Y., 1999. Vers une Neurogeometrie. Fibrations corticales, structures de contact et contours subjectifs modaux. Mathematiques, Informatique et Sciences Humaines, 1999, 145, EHESS, CAMS, Paris, pp. 5-101.

Priebe, N.J., Miller, K.D., Troyer, T.W., Krukowsky, A.E., 1998. Contrast-invariant orientation tuning in cat visual cortex: thalamocortical input tuning and correlation-based intracortical connectivity. J. Neurosci. 18, 5908–5927.

Rockland, K.S., Lund, J.S., 1982. Widespread periodic intrinsic connections in the tree shrew visual cortex. Science 215, 532–534.

Rockland, K.S., Lund, J.S., 1983. Intrinsic laminar lattice connections in the primate visual cortex. J. Comput. Neurol. 216 (3), 303318. May 20.

Sarti, A., Citti, G., Petitot, J., 2008. On the symplectic structure of the primary visual cortex. Biol. Cybernet. 98, 33–48.

Shelley, M., Wielaard, D.J., McLaughlin, D., Shapley, R., 2000. A neuronal network model of macaque primary visual cortex (V1): orientation selectivity and dynamics in the input layer $4C_\alpha$. PNAS 97, 8087–8092.

Worgotter, F., Koch, C., 1991. A detailed model of the primary visual pathway in the cat: comparison of afferent excitatory and intracortical inhibitory connection schemes for orientation selectivity. J. Neurosci. 11, 1959–1979.

Yen, Shih-Cheng, Finkel, L.H., 1998. Extraction of perceptually salient contours by striate cortical networks. Vision Res. 38 (5), 719–741.

ID	Title	Pages
2842450	Functional geometry of the horizontal connectivity in the primary visual cortex	9